Hybrid CFRP-BFRP Rebars for Prestress Concrete Slabs: Abaqus Analysis and Experimental Validation

Adam Ishag I[1] Arafa Juma Manis[2]

[1]*Department of Civil Engineering, Blue Nile University, Sudan (adam.ishag@yahoo.com)*

[2]*Department of Civil Engineering, Blue Nile University, Sudan*

https://doi.org/10.62049/jkncu.v4i1.74

Abstract

This study utilizes Abaqus finite element software to analyze concrete slabs reinforced with a novel hybrid of Carbon Fiber Reinforced Polymers (CFRP) and Basalt Fiber Reinforced Polymers (BFRP) rebars known as CBRP rebars. The investigation focuses on assessing the structural performance of these slabs under varying prestressing levels (PL) and FRP reduction factors (FR), along with the prestress index level (PI). The study defines the FR factor as the reduction in the transverse reinforcement area of FRP compared to the control slab. The PI is the ratio of prestressed CBRP rebars to the total FRP reinforcement in the transverse direction, aiming to determine a lower FRP reduction factor without compromising the FRP slabs' design requirements. Three FR values (0.45, 0.37, and 0.29) are considered, with the CBRP tendon tensioned at 35% and 50% of the ultimate strength, including 0.5 and 0.6 of the PI, for validation against experimental test data. The numerical analysis incorporates advanced finite element modeling techniques, integrating material properties, load conditions, and structural parameters to detail the behavior of CBR-reinforced concrete slabs. Various loading scenarios are simulated to evaluate the performance of CBRP rebars under diverse conditions. Comparison with experimental data validates the hybrid reinforcement approach's reliability. The study's findings contribute significantly to understanding the structural performance of concrete slabs reinforced with CBRP rebars. The hybridization of CFRP and BFRP rebars offers a promising alternative for enhancing concrete structure strength while reducing the carbon footprint associated with traditional reinforcement materials. The versatility of CBRP rebars allows customization based on specific structural requirements. Based on the Abaqus numerical analysis and its alignment with experimental data, the study recommends optimizing the CFRP-BFRP ratio to meet structural demands, evaluating long-term performance, and exploring environmental benefits associated with sustainable reinforcement materials. This research advances knowledge in the hybrid fiber-reinforced polymers field, offering insights for engineers and researchers seeking innovative solutions for concrete structure enhancement using Abaqus as a powerful analytical tool.

Keywords*:* Hybrid, CFRP, BFRP, Prestress, Slab, Abaqus, FEA

Introduction

Reinforced concrete has long been the cornerstone of modern construction due to its exceptional strength and ductility. The integration of various reinforcement materials has played a pivotal role in enhancing the performance and extending the service life of concrete structures. Among these materials, Carbon Fiber Reinforced Polymer (CFRP), Basalt Fiber Reinforced Polymer (BFRP), and Glass Fiber Reinforced Polymer (GFRP) rebars have emerged as promising alternatives to traditional steel reinforcement. The bridge slab reinforced with Fiber Reinforced Polymer (FRP) is widely investigated by many researchers (Michaluk, Rizkalla et al. 1998, Hassan, Abdelrahman et al. 2000, El-Salakawy and Benmokrane 2004, El-Ragaby, El-Salakawy et al. 2007, Pirayeh Gar, Head et al. 2013). Furthermore, in-situ for construction and design of FRP-RC bridge slabs was conducted in literature (Benmokrane, El-Salakawy et al. 2006, Ahmed, Settecasi et al. 2014). Due to low stiffness of FRP polymer, Reinforced concrete members reinforced with FRP have larger displacement and crack width among the steel reinforced concrete members.

The CFRP bars and GFRP bars was conducted in the previous studies. CFRP shows relatively high modulus of elasticity but high cost, but GFRP has relatively low costs nevertheless low modulus. To solve this issue, FRP hybrid composites was developed by numerous researchers (Bunsell and Harris 1974, Ali, Wang et al. 2014). They tested many specimens of basalt/carbon hybrid tendons to control the cost of carbon fiber by using BFRP with small loss of stiffness of the tendon (Ibrahim, Wu et al. 2016).

The incorporation of CFRP, BFRP, and GFRP rebars into concrete structures has gained significant attention due to their distinctive properties (Hajiloo, Green et al. 2017, Bilotta, Compagnone et al. 2020). CFRP offers remarkable tensile strength, corrosion resistance, and lightweight characteristics, making it an attractive choice for reinforcing concrete elements (ACI 440.2R-08 2008). BFRP, derived from natural basalt fibers, combines good mechanical properties with environmental sustainability, while GFRP provides excellent corrosion resistance and electromagnetic transparency. These alternative materials have the potential to address many of the limitations associated with traditional steel reinforcement, such as susceptibility to corrosion and magnetic interference, ultimately contributing to the longevity and sustainability of concrete structures.

FRP rebars can be used to reinforce concrete slabs in the same way as steel rebars. However, there are some important differences in the behavior of FRP-reinforced concrete slabs. For example, FRP rebars have a lower modulus of elasticity than steel rebars, which means that FRP-reinforced concrete slabs will deflect more under load. Additionally, FRP rebars are non-ductile, which means that they will fail suddenly without yielding.

Despite these differences, FRP-reinforced concrete slabs can be designed to meet the same performance requirements as steel-reinforced concrete slabs. FRP-reinforced concrete slabs have been successfully used in a variety of applications, including bridges, buildings, and marine structures.

A number of studies have been conducted to investigate the performance of CFRP, BFRP, and GFRP rebars in concrete slabs. The results of these studies have shown that FRP rebars can be used to successfully reinforce concrete slabs. However, it is important to note that the design and construction of FRP-reinforced concrete slabs require special considerations due to the different properties of FRP rebars compared to steel rebars.

Previous studies primarily focused on hybridizing carbon/PBO fibers with glass fibers to enhance structural performance and ductility, as seen in (Bakis, Nanni et al. 2001, Wu, Wang et al. 2007, Wang and Wu 2010). These studies emphasized the integration of carbon and glass FRPs to induce residual compressive stress in carbon fibers, avoiding damage localization and catastrophic failure. While some studies explored hybrid FRPs for structural strengthening, such as FRP tendons and sheets, little attention was given to the hybrid effect of carbon and basalt fiber rods (Tepfers, Tamužs et al. 1996, You, Park et al. 2007). Basalt fibers, known for higher strength, elastic modulus, and chemical stability compared to E-Glass FRP composites, when hybridized with carbon fibers, exhibited potential as an alternative material with superior behavior compared to glass fibers (Wang and Wu 2010). The concept of the "hybrid effect" has been widely studied, noting that the failure strain and strength of high modulus fibers in a hybrid composite tend to surpass those in pure high modulus fiber composites. However, both positive and negative hybrid effects can occur (Zweben 1977, Aveston and Kelly 1980, Kang, Kim et al. 2014). As infrastructure demands continue to grow and environmental concerns escalate, the development of innovative construction materials that reduce carbon emissions and enhance structural performance becomes increasingly vital.

This study will contribute valuable insights into the behavior of CFRP, BFRP, and GFRP rebars in reinforced concrete slabs, with a focus on their mechanical properties in various load conditions, and structural performance. By examining these key aspects, we aim to inform engineering practices and guide future decisions regarding the choice of reinforcement materials in construction projects, thereby advancing the field of sustainable and resilient infrastructure.

Finite Element Analysis

Finite Element Analysis (FEA) was carried out to investigate the concrete's contribution in tension and compression to simulate the cracking of reinforced concrete slabs and to compare the FEA results with the test data obtained. The commercial FEA software Program ABAQUS version 7-2023 (Abaqus 2011) was used for the present analysis. Concrete was modeled using three-dimensional 8-node solid elements C3D8, with three degrees of freedom for each node: translations u, v, and w in the three orthogonal directions x, y, and z, respectively. Steel reinforcement was modeled as discrete 3-D, 2-node truss elements with three degrees of freedom per node: u, v, and w. Perfect bond using an embedded region was assumed between the concrete and steel. Concrete damage plasticity (CDP) material was used according to the model of Milad (Hafezolghorani, Hejazi et al. 2017). The reinforcing FRP and tendons were modeled as embedded region reinforcement by rebar (truss) elements. One of the main features of embedded reinforcements is their ability to perform full bonding. In this study, a perfect bond between the FRP reinforcement and the adjacent material was assumed. The prestress of reinforcements was specified with a predefined field as stress, and the designated amount was applied in the FRP directions.

Material Properties

CDP was used to model concrete cracking in compression and tension. The smeared cracking approach was employed in this study to simulate the cracking of the RC slabs. FRP used as reinforcement rebars and FRP used as prestressed tendons were both modeled as elastic stiff materials. Three different types of reinforcement were used in this study, including steel, glass fiber reinforced polymer (GFRP), and carbon/basalt FRP (CFRP/BFRP) hybrid bars.

The mechanical properties of the steel, GFRP, and carbon/basalt hybrid rebars are listed in Table 1. The concrete strength of 30 MPa was obtained from concrete cubes after 28 days.

Table 1: Reinforcement Rebars Properties

Bar type	Diameter (mm)	Tensile strength (MPa)	Modulus of elasticity (GPa)	Ultimate strain (%)
Steel	12	400	200	0.2
Carbon-Basalt	10	1370	94	1.45
Carbon-Basalt	12	1370	94	1.45
GFRP	12	1170	48	2.40

Slab Geometry

Five slabs were simulated with Abaqus CAE software according to the tests. The slabs have a square shape with dimensions of 2400 mm in length and 200 mm in depth, and they are symmetric in the x and y directions as shown in Figure 1. The entire slab was modeled at full scale. For concrete meshing, the chosen element shape was Hex/Sweep, and mapping mesh was not selected, as depicted in Figure 2.

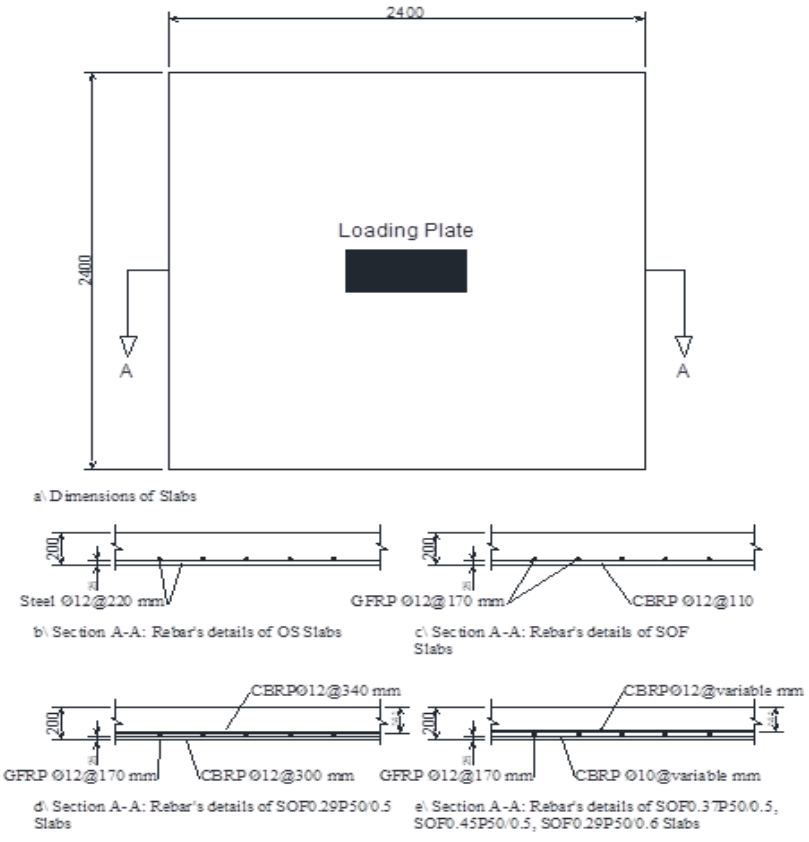

Figure 1 : Figure 1: Slabs Dimensions and Reinforcement Details

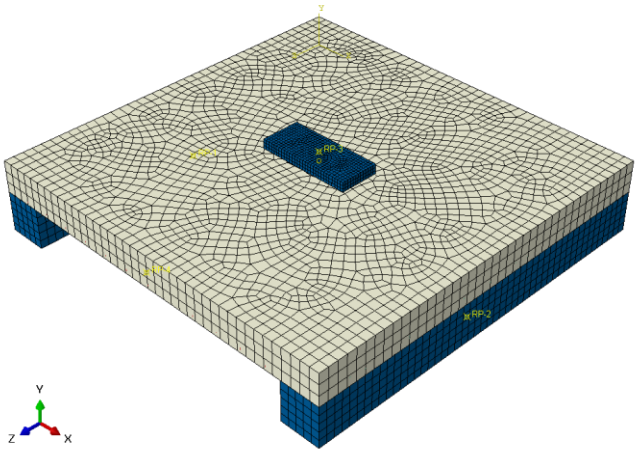

Figure 2: Mesh Details of Slabs

Figure 3 shows the slab setup for the FEA model, it is supported on two steel beams with dimensions of 250×250×2400 mm, one support is constrained as a hinge and the other is the roller. The loads were applied on top high tensile steel plate 600×250×20 mm mounted in the center of the slab. The slab setup in the testing machine is illustrated in Figure 4.

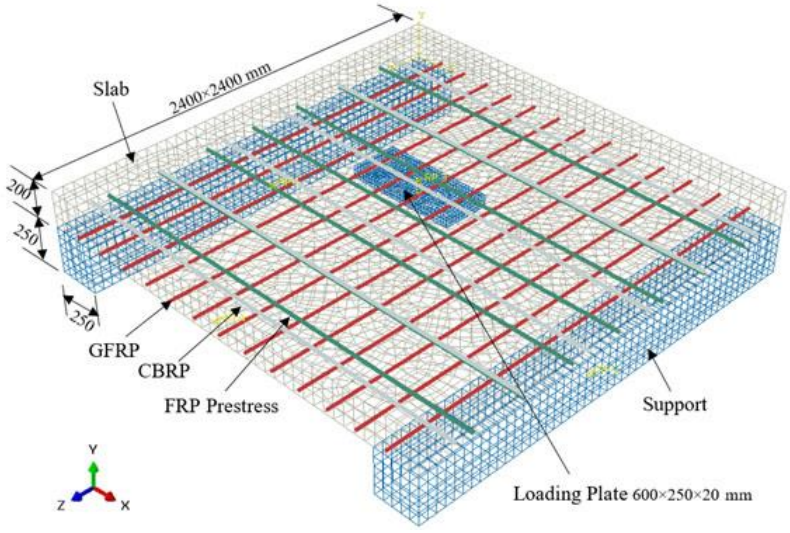

Figure 3: Shows Specimen Details and Mesh of the Simulated Slabs.

Figure 4: Photo of the Test Setup.

Five slabs were prestressed with CBRP hybrid tendons, including two slabs used as control slabs without prestressing. One of the control slabs was reinforced with ordinary steel (OS) rebars, with the bottom rebars designed according to the method outlined in the CSA-S6-06 (CSA) (2006) code. The OS slab was reinforced with steel rebars (Ø12@220mm, ratio 0.35%). The second control slab was reinforced with Ordinary Steel with FRP (SOF) and followed the aforementioned code. The longitudinal bottom rebars used GFRP rebars Ø12@110mm with a ratio of 0.40%, as illustrated in Figure 1. Additionally, this slab featured bottom transverse FRP bars of CBRP Ø12@110mm without prestressing.

The stressed slabs were configured based on three parameters: the prestressing level (PL%), the FRP reduction factor (FR), and the prestress index level (PI). The FR factor was defined as the reduction in the FRP transverse reinforcement area compared to the FRP-reinforced control slab. The PI was determined as the ratio of the prestressed CBRP rebars to the total FRP reinforcement in the transverse direction, with three values of FR (0.45, 0.37, and 0.29) employed. Furthermore, the CBRP tendon was tensioned to 35% and 50% of the ultimate strength, encompassing 0.5 and 0.6 of the PI.

All slabs were reinforced with GFRP rebars in the bottom longitudinal direction, serving as control slabs without top rebars, as outlined in Table 2. A concrete cover of 25 mm was maintained for all the specimens.

Table 2: Specimens Reinforcement Details

Specimen	$f'c$ **Mpa**	**Longitudinal Rebars**	**Transverse Rebars**		**Reduce Factor (FR)**	**Prestress Level (%)**	**Prestress Index Level (PI)**
			Prestressed	**Un-Prestressed**			
OS	25	Steel Ø12@220	N.A.	Steel Ø12@220	N.A.	N.A.	N.A.
SOF	27	GFRP Ø12@170	N.A.	CBRP Ø12@110	N.A.	N.A.	N.A.

SOF0.45P50/0.5	27	GFRP Ø12@170	CBRP Ø12@400	CBRP Ø10@300	0.45	50	0.50
SOF0.37P50/0.5	27	GFRP Ø12@170	CBRP Ø12@340	CBRP Ø10@65	0.37	50	0.50
SOF0.29P50/0.5	21	GFRP Ø12@170	CBRP Ø12@340	CBRP Ø12@300	0.29	50	0.50
SOF0.29P50/0.6	28	GFRP Ø12@170	CBRP Ø12@265	CBRP Ø10@265	0.29	50	0.60

Numerical Results and Discussion

The numerical results were presented based on the data obtained from the software, including load-displacement relationships, failure mode analysis, cracking loads, crack widths, displacement, strains in reinforcing bars and concrete, and ultimate capacity. To verify the FEA model against the test data, three slabs were utilized, reinforced with GFRP and a hybrid of Carbon/Basalt CBRP, employing both prestressed and un-prestressed approaches.

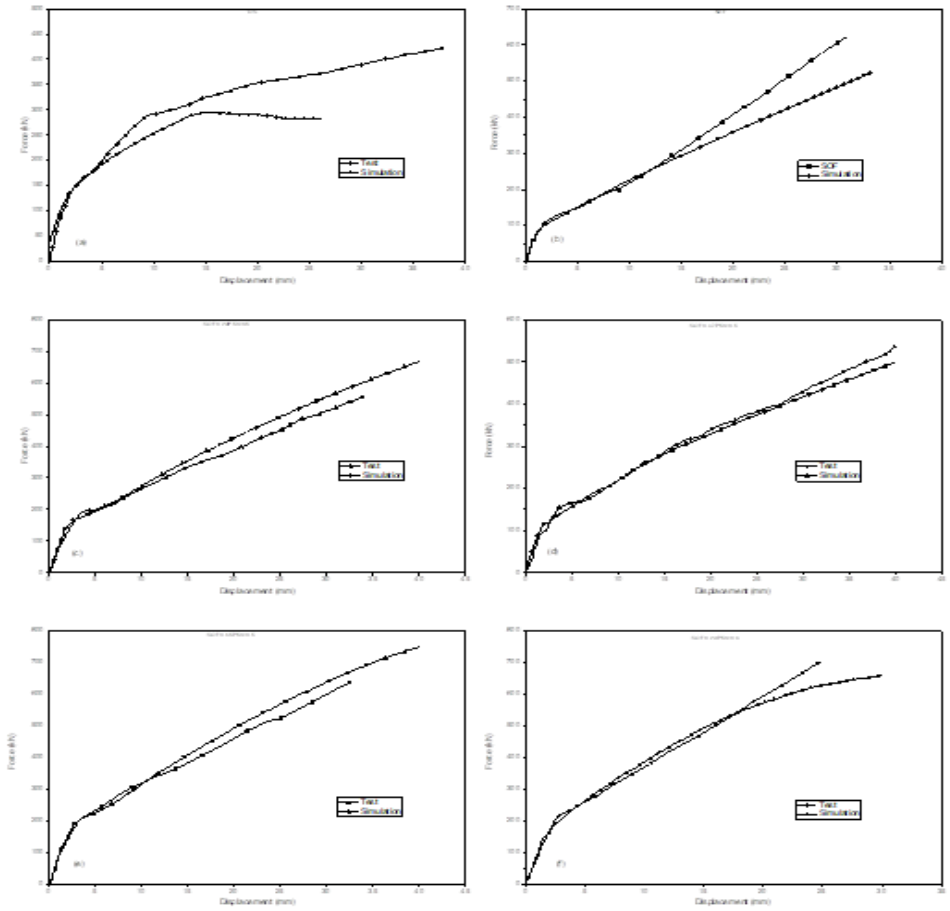

Figure 5: Load-Deflection Curves of the Experimental and FEA Simulation Results

Figure 5 (a – f) illustrates the comparison between the experimental and analytical load-deflection curves of the OS, SOF, SOF0.29P50/0.5, SOF0.37P50/0.5, SOF0.29P50/0.6, and SOF0.45P50/0.5 slabs. Discrepancies in the load-displacement between the OS and SOF slabs were observed, attributed to the assumption of the bond of the reinforcement made in the FEA simulation. However, the curve exhibited a good match with the test results up to a force of 300 kN. In the case of the prestressed slabs, the relationship between the simulation and test appeared to be similar, albeit with slight differences in the load-displacement behavior due to the assumptions regarding the bond of the FRP reinforcement and prestress with concrete. Notably, the FEA simulation did not account for the losses of the prestressed capacity.

For the SOF0.45P50/0.5 specimen, a significant change in the load-displacement was observed after yielding at a load of approximately 30 kN, which can be attributed to the loading steps.

The stiffness of the slabs was found to have varied depending on the amount of CBFP and the prestress level, as depicted in Figure 6. Nonetheless, the simulation was conducted based on displacement control, resulting in a slight observed drop in the load.

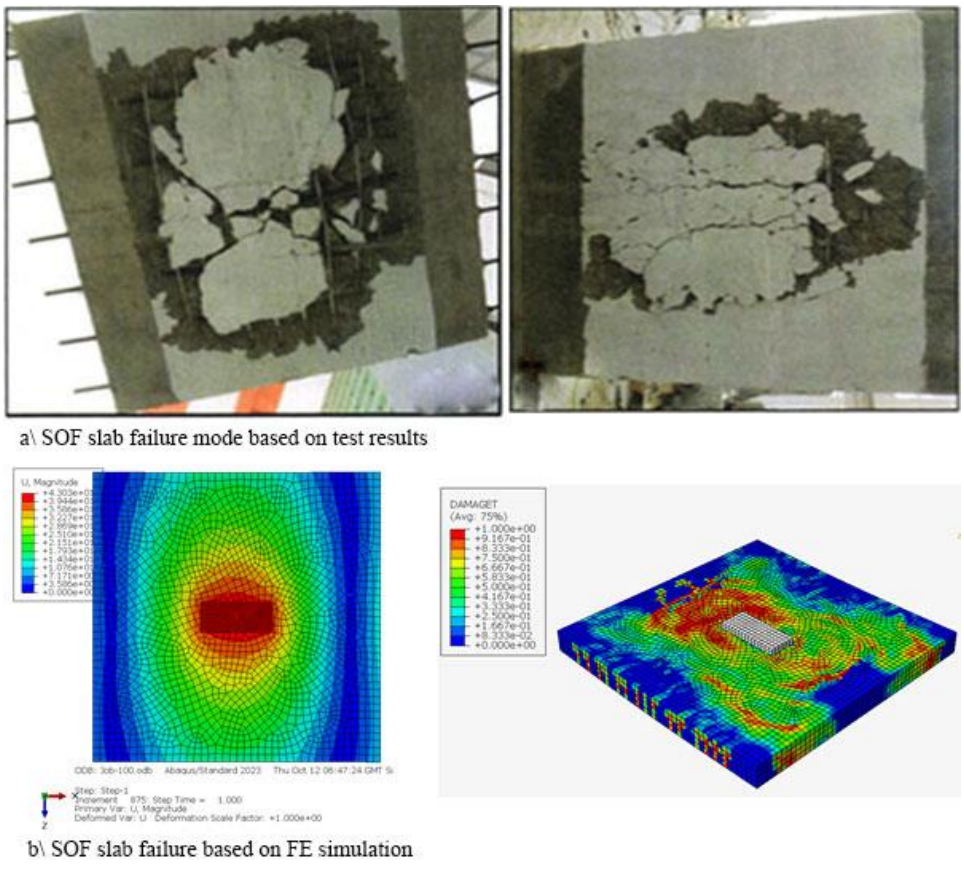

Figure 6: Comparison Between the Test and FEA Failure for SOF

Figure 6 shows a comparison between the test and FEA failure of the SOF and SOF0.37P50/0.5 slabs. The tension crack strain area for the prestressed slab appears to be larger than that of the un-prestressed slab, as evident from the test results, particularly in the damaged area on the bottom surface of the slab.

Furthermore, the ratio of the prestressed rebars to the total transverse reinforcement was defined as the prestressing index (PI). Three values of PI (20%, 35%, and 50%) were investigated and the results were compared to those of the un-prestressed slab.

Figure 6 presents the effect of the prestressing index on the tension crack at the bottom surface compared to the tested slabs. This figure demonstrates that the tension crack of the prestressed slabs is less pronounced than that of the un-prestressed slabs at the same load capacity. Moreover, an increase in the PI resulted in a reduced propagation of the tension crack at the bottom surface due to the initial compressive stresses beginning to counteract the tension cracks, thereby delaying their propagation.

Effect of Prestress Index Level

It seems like the study delves into the Influence of Prestressing Index level on slab performance. The research compared non-prestressed slabs to those with varying degrees of partial prestressing indices level (PI) 29%, 35%, and 50%. Notably, higher PI led to increased cracking load 108%, 191%, and 273% higher than the non-prestressed slab, respectively. However, the impact on the ultimate load was comparatively less 0.0%, 3.4%, and 10.7% increase, respectively. The deflection behavior exhibited similar trends before cracking, but after cracking, increased PI resulted in decreased deflection. Service load enhancement was observed 99%, 153%, and 203% increase for PI of 20%, 35%, and 50%, respectively. The tensile crack strains were lower in prestressed slabs compared to the non-prestressed slab, and higher PI reduced crack propagation due to initial compressive stresses countering tensile cracks, delaying their propagation.

Cracking Performance and Failure Mode

The cracking behavior and mode of failure were examined in test specimens where initial cracks appeared beneath the loaded area, initially parallel to supporting beams and slightly oriented away from the load Figure 6 (a, b). The extension of these cracks longitudinally depended on the transverse reinforcement ratio and prestressing level, with higher ratios or levels reducing crack extension outside the loaded area. Some slabs exhibited limited cracking under a certain load, prompting increased loading to induce additional cracks. Longitudinal cracks predominated up to near failure loads, leading to failure in punching or flexural/punching modes. Failure modes varied among slabs, with control slabs failing in flexural/punching mode and others failing in punching shear mode as shown in Figure 7. The top surface damage of prestressed slabs was larger than that of the FRP control slab, displaying different shapes such as elliptical or rectangular-like, notably affected by the load distribution beam as shown in Figure 6 (a, b), Figure 7. The bottom surface of tested slabs showed an approximately circular shape with a diameter equal to the spacing between girders. Notably, the non-prestressed transverse reinforcement exhibited severe fragmentation compared to prestressed tendons. This fragmentation could be linked to prestressed tendon debonding, causing stress distribution along their length. The control slab with higher reinforcement ratio displayed less fragmentation compared to prestressed slabs Figure 9, indicating a potential relationship between reinforcement ratio and fragmentation behavior.

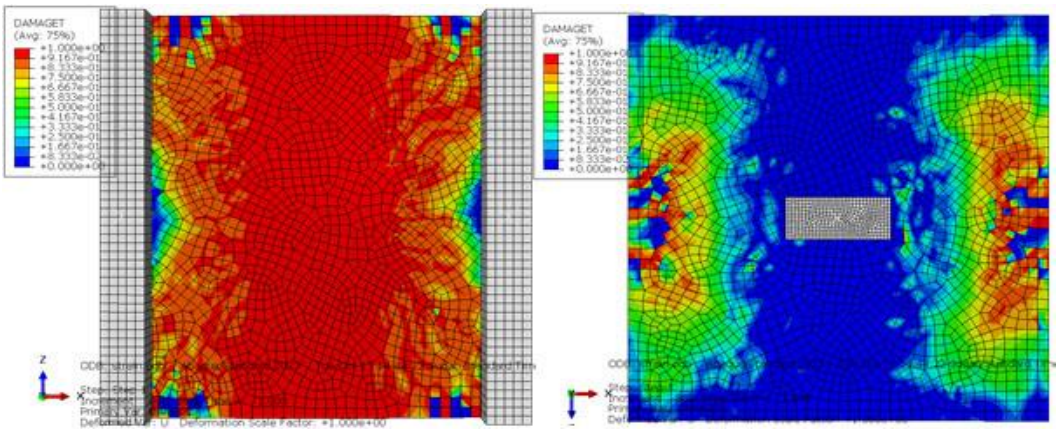

(a) (b)

Figure 7: Effect of prestressing index on (a) the tension crack at the bottom surface, and (b) compression crack at top surface of the slab

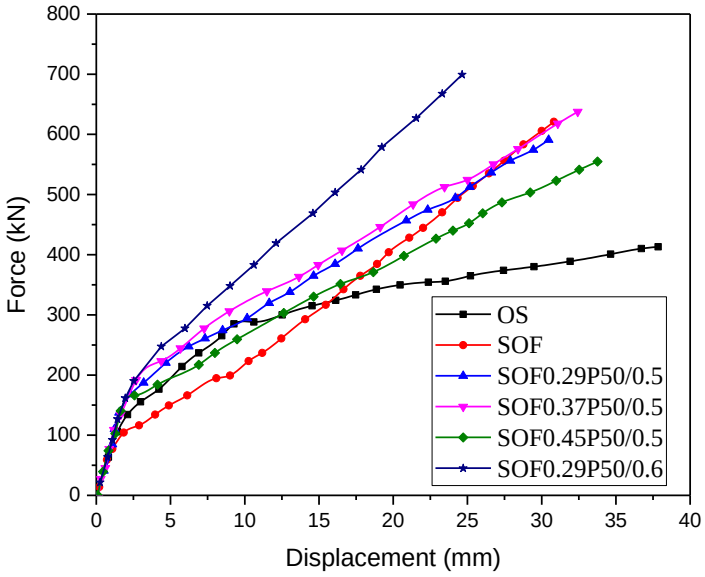

Figure 8: Load-Deflection for All Tested Slabs.

Figure 8 illustrates the load-displacement curves for the five slabs at the conclusion of the FEA simulation and the test. Linear performance was observed, and the deformation was consistent, regardless of the prestress level employed. Post-crack development, the deformation decreased with an increase in the prestress level. The service load, cracking load, and ultimate load of the prestressed slabs were higher than those of the slabs cast without prestressing. Additionally, slabs with a 35% PI exhibited cracking loads that were 120% and 195% higher than those of the 35% and 50% prestress level slabs, respectively. Slabs with a 50% PI demonstrated an increased cracking load of 30% and 50%, resulting in 175% and 270% of the respective prestress levels.

Therefore, the deflection behavior analysis encompassed load-maximum displacement curves, highlighting the influence of factors like FRP reduction factor, prestressing level, and partial prestressing index. The load- displacement curves for FRP-reinforced/prestressed concrete slabs exhibited bilinear behavior, representing un-cracked and cracked slab phases. In contrast, the steel-reinforced control slab displayed

linear behavior until the cracking load, followed by nonlinear behavior due to concrete cracking and steel reinforcement yielding. Post-cracking stiffness varied among FEA and tested slabs, affected by reinforcement area and prestress level variations. Despite different behaviors, displacement at the service load level remained within allowable limits. The study noted that certain prestressed slabs displayed cracking loads higher than the service load level, hence governed by the concrete cross-section's inertia. Moreover, the residual displacement, particularly affected by prestressing force, were lower in FRP-prestressed slabs compared to steel-reinforced slabs. Increasing prestressing level significantly reduced residual displacement. Additionally, displacement profiles indicated different behavior between steel and FRP-reinforced control slabs, with the latter showing sharper slopes due to the lack of yielding in FRP reinforcement.

Therefore, FRP-prestressed reinforced slabs with specific FRP reduction factors and prestressing levels not only exhibited displacement within permissible limits but also displayed superior behavior compared to non-prestressed FRP- reinforced control slabs.

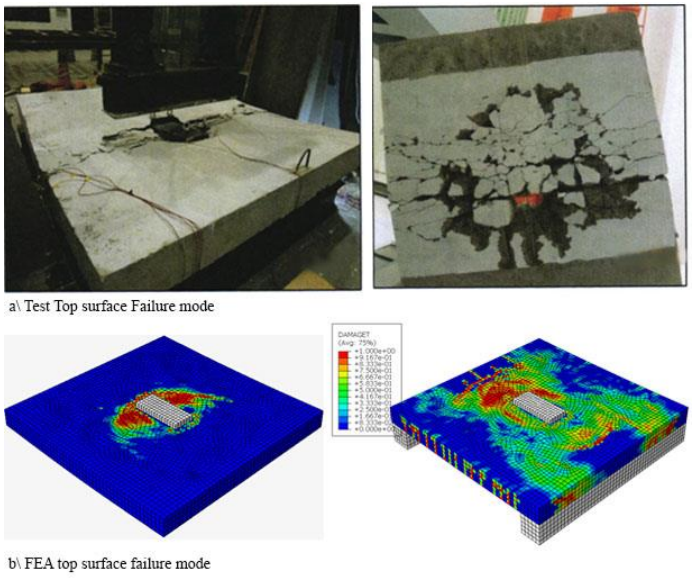

Figure 9: Failure Mode and damage of SOF slab

Effect Top Reinforcement

In this study, no top reinforcement rebars were used in the slab direction. Top reinforcement rebars with a ratio of 0.3% GFRP were employed in the longitudinal and transverse directions, in accordance with the Canadian Highway Bridge Design Code (Canadian Standards Association (CSA) 2019). The failure load for the slab without top rebars was 790 kN. The inclusion of top rebars with a ratio of 0.3% GFRP increased the failure mode by 7%. Consequently, the small ratio for the top rebars did not significantly impact the ultimate capacity or serviceability of the slab.

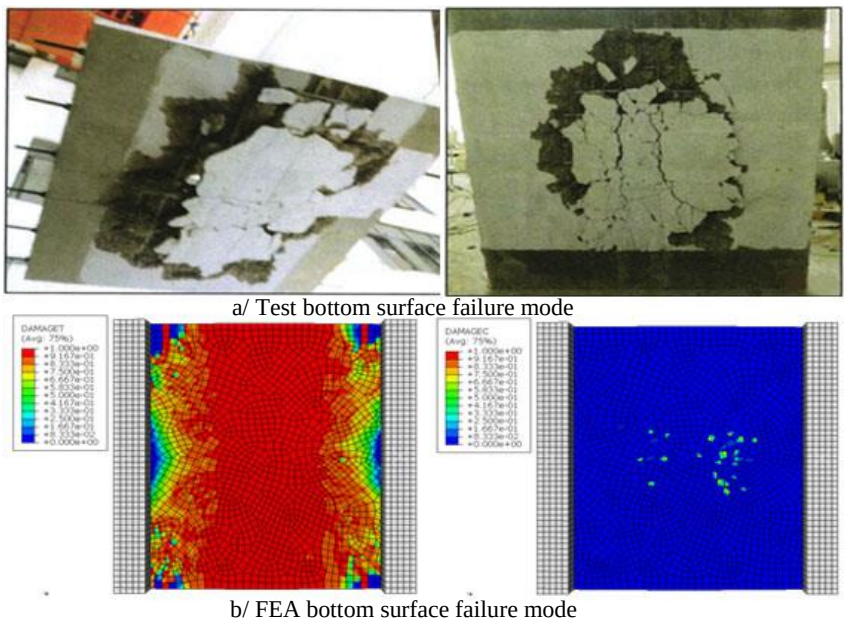

a/ Test bottom surface failure mode

b/ FEA bottom surface failure mode

Figure 10: Failure Mode and Damage of SOF0.45P50/0.5 Slab at Bottom Surface

Conclusion

The comprehensive numerical analysis and experimental investigation of concrete slabs reinforced with a novel hybrid of Carbon Fiber Reinforced Polymers (CFRP) and Basalt Fiber Reinforced Polymers (BFRP) rebars, referred to as CBRP rebars, have provided valuable insights into the structural performance and behavior of these materials. The study demonstrated the significant influence of various parameters, including prestressing level (PL), FRP reduce factor (FR), and prestress index (PI), on the overall performance of the slabs.

The findings underscored the potential of the hybrid CFRP-BFRP rebars in enhancing the strength of concrete structures while simultaneously reducing the carbon footprint associated with traditional reinforcement materials. The study highlighted the feasibility of utilizing these advanced composites in concrete slabs, offering promising alternatives to conventional steel reinforcement.

Additionally, the investigation revealed the importance of the prestressing index (PI) in controlling tension crack propagation and enhancing the load-bearing capacity of the slabs. The application of a higher PI was observed to effectively delay the propagation of tension cracks and improve the overall performance of the slabs.

Furthermore, the incorporation of top reinforcement rebars with a small ratio of 0.3% GFRP did not significantly affect the ultimate capacity or serviceability of the slabs, indicating the potential for cost-effective reinforcement solutions in practical applications.

Deflection behavior analysis showcased the load-deflection characteristics of different slabs, emphasizing the bilinear nature of FRP-reinforced/prestressed concrete slabs compared to the linear behavior of steel-reinforced control slabs. Prestressed slabs displayed reduced residual deflections compared to their non-prestressed counterparts, indicating the influence of prestressing force on mitigating deformations.

Analysis of failure modes revealed that the behavior of the slabs differed depending on reinforcement types and prestressing levels. The observed failure modes varied between flexural/punching and punching shear modes, with different slabs displaying distinct patterns of cracks and damage propagation.

Overall, this research contributes to the understanding of hybrid fiber-reinforced polymers' behavior in concrete structures, emphasizing the importance of tailored design considerations to optimize the structural performance and strength of concrete slabs. The study's insights are expected to guide future engineering practices and promote the adoption of sustainable and resilient construction materials in the building industry.

References

Abaqus, G. (2011). *Abaqus 6.11*. Providence, RI, USA: Dassault Systemes Simulia Corporation.

ACI 440.2R-08. (2008). *Guide for the design and construction of concrete reinforced with FRP bars*. Detroit: American Concrete Institute (ACI).

Ahmed, E. A., et al. (2014). Construction and testing of GFRP steel hybrid-reinforced concrete bridge-deck slabs of Sainte-Catherine overpass bridges. *Journal of Bridge Engineering, 19*(6), 04014011.

Ali, N. M., et al. (2014). Integrated performance of FRP tendons with fiber hybridization. *Journal of Composites for Construction, 18*(3), A4013007.

Aveston, J., & Kelly, A. (1980). Tensile first cracking strain and strength of hybrid composites and laminates. *Philosophical Transactions of the Royal Society of London. Series A, Mathematical and Physical Sciences, 294*(1411), 519-534.

Bakis, C., et al. (2001). Self-monitoring, pseudo-ductile, hybrid FRP reinforcement rods for concrete applications. *Composites Science and Technology, 61*(6), 815-823.

Benmokrane, B., et al. (2006). Designing and testing of concrete bridge decks reinforced with glass FRP bars. *Journal of Bridge Engineering, 11*(2), 217-229.

Bilotta, A., et al. (2020). Structural behaviour of FRP reinforced concrete slabs in fire. *Engineering Structures, 221*, 111058.

Bunsell, A., & Harris, B. (1974). Hybrid carbon and glass fibre composites. *Composites, 5*(4), 157-164.

Canadian Standards Association (CSA). (2019). Design and Construction of Concrete Structures Reinforced with Fibre-Reinforced Polymers. Mississauga, ON: CSA. 33, 521-534.

El-Ragaby, A., et al. (2007). Fatigue life evaluation of concrete bridge deck slabs reinforced with glass FRP composite bars. *Journal of Composites for Construction, 11*(3), 258-268.

El-Salakawy, E., & Benmokrane, B. (2004). Serviceability of concrete bridge deck slabs reinforced with fiber-reinforced polymer composite bars. *Structural Journal, 101*(5), 727-736.

Hafezolghorani, M., et al. (2017). Simplified damage plasticity model for concrete. *Structural Engineering International, 27*(1), 68-78.

Hajiloo, H., et al. (2017). Fire tests on full-scale FRP reinforced concrete slabs. *Composite Structures, 179*, 705-719.

Hassan, T., et al. (2000). Fibre reinforced polymer reinforcing bars for bridge decks. *Canadian Journal of Civil Engineering, 27*(5), 839-849.

Ibrahim, A. I., et al. (2016). Experimental Study of Cyclic Behavior of Concrete Bridge Columns Reinforced by Steel Basalt-Fiber Composite Bars and Hybrid Stirrups. *Journal of Composites for Construction, 04016091.

Kang, T. H.-K., et al. (2014). Hybrid effects of carbon-glass FRP sheets in combination with or without concrete beams. *International Journal of Concrete Structures and Materials, 8*(1), 27-41.

Michaluk, C. R., et al. (1998). Flexural behavior of one-way concrete slabs reinforced by fiber reinforced plastic reinforcements. *Structural Journal, 95*(3), 353-365.

Pirayeh Gar, S., et al. (2013). Comparative experimental performance of bridge deck slabs with AFRP and steel precast panels. *Journal of Composites for Construction, 17*(6), 04013014.

Tepfers, R., et al. (1996). Ductility of nonmetallic hybrid fiber composite reinforcement for concrete. *Mechanics of Composite Materials, 32*(2), 113-121.

Wang, X., & Wu, Z. (2010). Evaluation of FRP and hybrid FRP cables for super long-span cable-stayed bridges. *Composite Structures, 92*(10), 2582-2590.

Wu, Z., et al. (2007). State-of-the-art of advanced FRP applications in civil infrastructure in Japan. *Composites and Polycon, 37*, 1-17.

You, Y.-J., et al. (2007). Hybrid effect on tensile properties of FRP rods with various material compositions. *Composite Structures, 80*(1), 117-122.

Zweben, C. (1977). Tensile strength of hybrid composites. *Journal of Materials Science, 12*, 1325-1337.